Measuring Total Filtration Efficiency of Surgical and Community Face Masks: Impact of Mask Design Features

Silvia Chiera, Alessandro Cristoforetti, Luca Benedetti, Luca Borro, Lorenzo Mazzei, Giandomenico Nollo, Alessio Bucciarelli, and Francesco Tessarolo

***Abstract*— Surgical and community face masks are used worldwide to reduce the transmission of respiratory infections in indoor environments. Performance parameters for these loose-fitting devices are mainly focused on material filtering efficiency, while, differently from face respirators, there are no standard methods for measuring the fraction of air leaking at the face seal. This study quantifies the total filtration efficiency (TFE), a parameter based both on filter efficiency and air leakage, of 50 face mask models with the aim of understanding the role of several mask design features on TFE performance. An instrumented head form equipped with sensors for measuring volumetric airflow and differential pressure was used to simulate the air exhalation from the mouth of a person wearing a face mask. A response surface method (RSM) was used to model the TFE experimental data. Results showed that TFE values ranged over a wide interval (from 5% to 73%), with better values at higher flow rates. A significant positive correlation was found between TFE and filter breathability. The presence of a nosepiece (NP) showed to increase the TFE on average from 4% to 6%, according to the flow rate. Significant improvements were associated only to nosepieces incorporating a metallic wire. The RSM model evidenced that the increase in the number of the filter layers and the use of a meltblown layer result in higher TFE only when a nosepiece is in place. Differently, the benefit of the nosepiece is less marked for masks made of highly breathable filters. To improve overall mask performance, the design of loose-fitting face masks should carefully compromise between breathability and filtration efficiency of the filter materials. The addition of a metallic nosepiece helps improving the TFE by limiting the air leaking at the face seal.**

***Index Terms*— Breathability, COVID-19, differential pressure (DP), face masks, face seal, filtration efficiency (FE), mask design, nosepiece (NP), response surface method (RSM), SARS-CoV-2.**

I. Introduction

THE main route of transmission of SARS-CoV-2 is through inhalation in the upper airways of the aerosols and saliva's droplets generated by respiration, sneezing, and coughing [1], [2], while contact with contaminated surfaces plays a minor role [3], [4]. The use of face masks to cover mouth and nose consequently proved to be among the most effective tools for limiting the spread of SARS-CoV-2 [5]. Recent studies confirmed that the pandemic could be significantly limited by the correct and widespread use of a face mask among the population [2], [6] with particular attention to the correct use and fitting of the masks [7]. Based on these findings, specific recommendations and regulations for the population about face mask use were enforced in many countries [8], [9]. Because of the sudden increase in demand for face masks and the resulting failure of the supply chain [10], new products entered the market exploring alternative systems and materials for protecting the nose and the mouth from potentially SARS-CoV-2 contaminated droplets and aerosol [11]. To create a distinction from medically certified devices (usually identified as "medical" or "surgical" masks), new terms like "homemade masks" [12], [13] or "community masks (CMs)" [14] were adopted for all face mask products that were not meeting the performance and safety standards of medical masks or were not tested for.

In the rapidly evolving context of the COVID-19 pandemic, the World Health Organization published an interim guidance [15] underlying that filtration efficiency (FE), breathability, and face fit are essential characteristics to be considered for all type of face mask in order to guarantee their safety and efficacy.

Unfortunately, the European Standard EN 14683:2019 [16] for surgical mask (SM) and the American Society for Testing and Materials (ASTM) standard for medical masks [17] indicate minimal requirements for bacterial filtration efficiency

Manuscript received 14 October 2022; revised 20 February 2023; accepted 26 February 2023. Date of publication 15 March 2023; date of current version 24 March 2023. This work was supported by the "Laboratorio Associato COrona VIrus Disease (COVID)-19 (LASS) Project" of the University of Trento through internal grant "Bando interno 2020 Università di Trento COVID 19." The work of Francesco Tessarolo was supported by the European Union—Fondo Sociale Europeo Recovery Assistance for Cohesion and the Territories of the European Union (FSE-REACT-EU), Programma Operativo Nazionale (PON) Research and Innovation 2014–2020, under Grant DM 1062/2021. The work of Alessio Bucciarelli was supported by Istituto di Ricovero e Cura a Carattere Scientifico (IRCCS) Istituto Ortopedico Rizzoli (Ricerca Corrente). The Associate Editor coordinating the review process was Dr. Priya Ranjan Muduli. *(Silvia Chiera and Alessandro Cristoforetti are co-first authors.) (Corresponding author: Francesco Tessarolo.)*

Silvia Chiera, Luca Benedetti, Giandomenico Nollo, and Francesco Tessarolo are with the Department of Industrial Engineering, University of Trento, 38123 Trento, Italy (e-mail: silvia.chiera@unitn.it; luca.benedetti@unitn.it; giandomenico.nollo@unitn.it; francesco.tessarolo@unitn.it).

Alessandro Cristoforetti is with the Department of Cellular, Computational and Integrative Biology (CIBIO), University of Trento, 38123 Trento, Italy, and also with the Department of Information Engineering and Computer Science (DISI), University of Trento, 38123 Trento, Italy (e-mail: alessandro.cristoforetti@unitn.it).

Luca Borro is with the Imaging Department/3DLaboratory, Bambino Gesù Children's Hospital, 00146 Rome, Italy (e-mail: luca.borro@opbg.net).

Lorenzo Mazzei is with Ergon Research, 50127 Florence, Italy (e-mail: lorenzo.mazzei@ergonresearch.it).

Alessio Bucciarelli is with the Laboratorio RAMSES, IRCCS Istituto Ortopedico Rizzoli, 40136 Bologna, Italy (e-mail: alessio.bucciarelli@ior.it).

This article has supplementary downloadable material available at https://doi.org/10.1109/TIM.2023.3257326, provided by the authors.

Digital Object Identifier 10.1109/TIM.2023.3257326

(BFE) and differential pressure (DP) but do not provide any methods or equipment to assess the fit on user's face or to quantify the air leaking at the face seal.

Regarding the performance standards of CMs, at present, no mandatory regulation exists, while only a discretionary guide to minimal requirements has been made available by the European Committee for Standardization [14]. ASTM has recently provided a framework for the specifications of barrier face covering performance [18]. However, the document recognizes that no accepted methodologies were defined to measure total filtration efficiency (TFE) from loose-fitting face masks and face coverings despite recent studies have demonstrated the relation of mask design features and fitting with air leakage and overall filtration performance [19], [20], [21], [22].

The quantification of the FE of surgical and community face masks should be based on the analysis of the two pathways for the exhaled air: leakage through the face seal and flow through the filter [23]. These combined effects involve complex airflow phenomena, and, while during the process of inhalation the DP facilitate the sealing of a reasonably well-fit mask [24], it is during exhalation that the increased inner pressure pushes the mask away from the face, inducing higher perimetral leakage [25], [26]. The perfect mask seal for loosely fitting masks, such as SM and CM, is only ideal, and significant leakage at the face seal has been reported in the literature for a range of mask models by several authors [27], [28], [29]. Apart from mask design and material characteristics, leakage at the face seal can be affected by a number of other factors and is highly user-dependent. In fact, facial size and anthropometric features were shown to have an impact on fit and leakage [30], and variability in user compliance with the indications for use in donning a face mask was shown to dramatically modify the fraction of air leaking at the mask perimeter [27].

Differently from inward protection, which can be determined by established standard mask fit tests, the flow physics of outward protection is a far less studied phenomenon, both experimentally and computationally [31], [32], [33]. Person-to-person variability and the effect of the expiratory particle size on FE are further aspects in need of scrutiny [34]. As shown by prepandemic studies, given the relevant number of particles that can pass through the face seal, establishing an optimal fit should be of upper importance during mask development, to minimize face seal leakage [23]. To complete the characterization of the overall efficacy of SM and CM, it is then urgent to integrate the FE of the filtering material with the quantification of the fraction of exhaled air leaking at the face seal. Additionally, the accurate evaluation of protection efficiency of face masks should direct improvements to their design and inform guidelines about their usage [24]. A large interest remains, even after the pandemic peak, in educating the population about the correct use of personal protective equipment for preventing respiratory infections [21], spurring the research on simple performance metrics to predict the impact of materials and designs on mask efficiency [35].

Several studies evidenced the importance of evaluating the airflow leaking from face masks since the unfiltered air exhaled by an infected person can play a critical role in virus transmission [20]. However, most of the experiments performed to study the ability of face masks at containing the viral spread relied on qualitative tests, showing leak flow preferential direction, droplet projection distance, or aerosol density distribution [6], [20], [23], [29], [36], but without providing numbers on the fraction of air leaking at the face seal. More recently, the fraction of the respiratory droplets and aerosol blocked by cloth masks was measured by Lindsley et al. [35] and coworkers, using a setup that included a realistic head form, a large aerosol chamber, and a multistage aerosol impactor. Further experimental studies, in vivo, in vitro using manikins, and in silico, evidenced the importance of considering material breathability combined with mask design factors, revealing the role of the fit of the mask in impacting the filtering efficiency [30], [37], [38]. Ipaki et al. [30] proved how face anthropometry can influence the fitting, suggesting a redesigning of face mask parameters by adjusting leakage critical points with a paper prototype fit on the user's face. Wang et al. [37] and Solano et al. [38] studied how leakages were linked to a wide variety of facial characteristics and mask designs using a 3-D-scanning face model. Further studies on face mask fitting were also conducted with finite-element analysis and aimed at studying the contact pressure between mask and facial anatomy [39]. Additive manufacturing (AM) was investigated in silico by Carr et al. [19] as a mean to optimize fitting and reduce leakage, obtaining an effective sealing only by filling the gap between the mask and the face with an adaptable gasket added to the rigid AM materials. Breathability, dependent on the mask filtering material characteristics, also emerged as an important parameter influencing mask FE via its strong causal relationship with leakage [27], [40].

The accuracy and reproducibility of both leakage and breathability measurements need to be investigated further in relation to the experimental errors [41], [42]. Since there is a lack of information on how the intrinsic variability among mask samples could affect measurement uncertainty, replicated measurements appear the most reliable experimental approach to estimate the confidence of any newly introduced mask performance parameter. This strategy has been pursued in previous pilot studies by Chiera et al. [27], [43] for measuring leakage and the TFE, mainly focusing on the influence of wearing styles and mask breathability on the overall mask performance.

This study is aimed at applying a recently developed method to quantify the outward TFE on a wide range of SM and CM, not only to extend the evaluation of filtration performance on a more comprehensive number of face covering products and grabbing a clearer view about TFE measurement uncertainty and variability, but also with the goal of understanding the role of several mask design parameters and filter properties on TFE, providing evidence-based indications for the design and fabrication of more efficient face masks.

II. Materials and Methods

In this study, to determine the mask TFE, we exploited the method for the quantification of the leakage fraction of face masks we recently developed in [27]. The method is based on an instrumented head form equipped with sensors

for measuring volumetric airflow and DP. Details of the test rig, the theoretical model, and the data analysis process are detailed in [27] and summarized here.

A. Theoretical Model

In real conditions, where the face fit of the mask is not perfect, the total airflow $Q_{\text{I tot}}$ exhaled by the mouth splits into two components, $Q_{\text{I mask}}$ passing through the mask filter and the $Q_{\text{I leak}}$ leaking through the mask boundaries

$$Q_{\text{I tot}} = Q_{\text{I mask}} + Q_{\text{I leak}}. \tag{1}$$

The resistance created by the face mask materials and design to the exhaled airflow determines the DP ΔP_{I} between the inside of the mask and the external environment, which is the common driver for both $Q_{\text{I mask}}$ and $Q_{\text{I leak}}$. This DP is also linked to the breathability of the mask since lower ΔP_{I} values facilitate the mask user's breathing. By definition, $Q_{\text{I mask}}$ is only determined by the resistance $R_{\text{I mask}}$ of the mask filter. According to Darcy's law [44], the volumetric flow rate of a fluid with a viscosity μ through the porous medium having a cross-sectional area A, a thickness L, and a permeability k is proportional to pressure drop applied across the porous medium [45]. This allows modeling the flux through the mask material as

$$\Delta P_{\text{I}} = Q_{\text{I mask}} \cdot R_{\text{I mask}} \tag{2}$$

where $R_{\text{I mask}}$ is related to the filter permeation characteristics as follows:

$$R_{\text{I mask}} = \mu \text{L/kA}. \tag{3}$$

Differently from $Q_{\text{I mask}}$, $Q_{\text{I leak}}$ cannot be simply modeled or calculated since the resistance of the airflow escaping from the mask seal is related both to flow velocity and turbulence, and the size and shape of the openings at the face seal interface.

In order to obtain separate measurements for the components $Q_{\text{I mask}}$ and $Q_{\text{I leak}}$, we devised a two-phase experimental protocol which included measurements in the ideal experimental condition where no air leak was present (perfect mask fit to the face). This condition is described by a flux model where the total airflow is represented only by the flow passing through the mask $Q_{\text{II mask}}$, which can be related to the mask resistance $R_{\text{II mask}}$ and the DP ΔP_{II} measured in ideal condition by the following equation, similar to (2):

$$\Delta P_{\text{II}} = Q_{\text{II mask}} \cdot R_{\text{II mask}}. \tag{4}$$

B. Experimental Setup

The TFE calculation was based on the measurement of the $Q_{\text{I mask}}$ fraction of the exhaled air performed with an experimental setup based on a polylactic acid dummy head. A comprehensive view of the experimental setup is presented in Fig. 1. The dummy head was 3-D-printed according to the dimensional characteristics of the medium-sized head, as specified by the standard ISO 16900-5 [46]. The porosity of the surface was reduced by sandpaper and epoxy resin finishing.

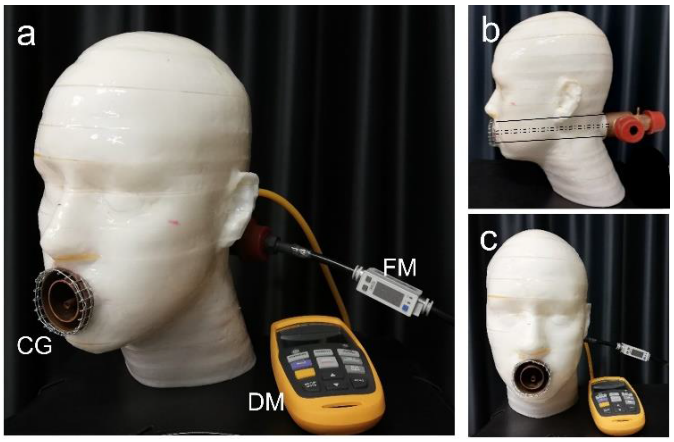

Fig. 1. Experimental setup for the measurement of face masks leak fraction: (a) dummy head instrumented with the pipe system, the outlet CG, the connected DM, and the compressed air supply equipped with the FM; (b) side view, indicating the inner piping connecting the mouth opening with the airflow inlet and the DP manometer; and (c) front view of the setup. Reprinted with permission from [43].

The head form was then instrumented with a pipe system which conveyed a controlled airflow from a compressed air supply to the mouth region, as specified in part 8.9 of the EN 149:2009 standard [47]. The outlet of a 42-mm-diameter tube, devoted to simulating air inhalation (not used in this study), was present at the mouth region. Air exhalation was instead simulated by an inner concentric tube of 28 mm in diameter. The pressure at the center of the mouth opening was sampled by using a differential manometer (DM), referred to environmental pressure, connected to the mouth by a third smaller tube (6 mm in diameter). Exhalation was mimicked by a constant airflow generated by the compressed air supply through the 28-mm tube, measured by a dedicated flowmeter (FM). A circular grid (CG) placed on the mouth opening prevented direct contact between the outlet and the mask surface, allowing a homogeneous spread of the flow outside the mouth even when the ear loops tightly pressed the mask on the dummy head.

The airflow values specified for testing face respirators according to the standards [17], and typically generated during speech [49], were reproduced in this study by generating an airflow rate between 30 and 160 L/min. The airflow rate exiting the dummy head in steady-state conditions was measured by a digital flow sensor (Digital Flow Switch PFM7, SMC Corporation, Tokyo, Japan) claiming an accuracy of 3% of the read value [+1 least significant digit (LSD)] and a resolution of 1 L/min for air at 25 °C in the 2–200-L/min measuring range. The DP ΔP, occurring between the dummy head mouth opening and the exterior environment, was measured by a DM (Fluke 992, Fluke Corporation, Everett, WA, USA), claiming an accuracy of 1% of the read value (+1 LSD) and a resolution of 1 Pa in the 1–4000-Pa measuring range. Both the FM and the DM were calibrated from the manufacturer, and study measurements were collected within one year from calibration date. Deviations from the volumetric airflow measurement due to shift of environmental temperature (21 ± 2) °C from nominal working temperature and possible differences in pressures occurring at different experimental phases were negligible (<0.1%).

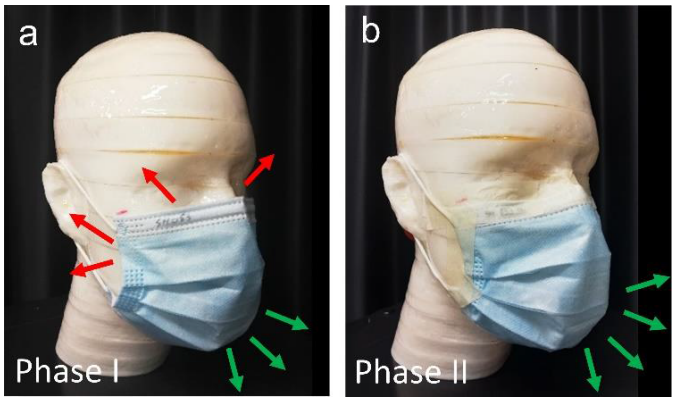

Fig. 2. Face mask mounted on the head form during the two different phases of the experimental protocol: (a) phase I of the experiment and (b) phase II of the experiment. Note the adhesive tape used for sealing the gap at face–mask interface during phase II of the experiment. The superimposed arrows conceptualize the exhaled airflow passing through the leaks (red arrows) and through the mask (green arrows). Reprinted with permission from [43].

C. Experimental Protocol

The experiment consisted of two phases corresponding to different modalities of applying the mask to the face dummy (Fig. 2). Their comparison allowed separating and quantifying the exhaled airflow components passing through the mask filter and leaking through the boundary.

The first phase (Phase I) emulated the real situation of wearing a mask, where leaks are present and no extra means were applied to set the mask in place [Fig. 2(a)]. The positioning of the tested masks on the dummy head followed manufacturer's instruction for use (IFU), covering both nose and mouth, hanging the ear laces at their intended position, and applying fingers pressure to conform the mask border as much as possible to the dummy head surface. Whenever present, the nosepiece (NP) was also carefully adapted to the nose ridge profile to optimize the mask seal.

With the mask properly positioned, constant airflow rates $Q_{\mathrm{I\,tot}}$ were generated from the air supply, and when reaching a steady-state condition (5 s after reading the expected airflow rate on the FM), the corresponding values of DP ΔP_{I} were collected on the DM. The procedure was performed for $Q_{\mathrm{I\,tot}}$ equal to 30, 90, and 160 L/min, as they were considered representatives for low, medium, and high flow rates during real breathing conditions.

The second phase (Phase II) of the experiment mimicked the ideal situation of a perfect mask fit, where no leak is present, and the entirety of the exhaled airflow passes through the mask filter. To achieve this condition, after the mask was fit on the dummy head according to the same procedure of Phase I, the mask boundaries were hermetically sealed on the dummy surface using adhesive tape (paper masking tape, 25 mm width, Tesa[1] Masking Economy, Tesa SE, Hamburg, Germany), avoiding in this way any air leakage [Fig. 2(b)]. The tape was applied on the peripheral welded areas of the mask that do not contribute to air filtering, ensuring the absence of any residual gap by visual inspection of tape adherence both before and after each measurement. Several steady-state airflow rates, indicated as $Q_{\mathrm{II\,mask}}$, were generated in these experimental conditions, and the corresponding set of DP measurements, indicated as ΔP_{II}, was collected. In Phase II, $Q_{\mathrm{II\,mask}}$ varied from 30 to 160 L/min, at increments of 10 L/min.

[1]Trademarked.

D. Data Analysis

The measurements of $Q_{\mathrm{I\,tot}}$ and ΔP_{I} obtained in the realistic conditions of Phase I do not allow separating the fraction of leaked airflow from the total airflow in (1) since the separate contributions of filter ($R_{\mathrm{I\,mask}}$) and seal to overall mask resistance are unknown. However, in the experimental conditions of Phase II, values of $R_{\mathrm{II\,mask}}$ were determined by using (4) for 14 measurements of ΔP_{II} and $Q_{\mathrm{II\,mask}}$ (every 10 L/min in the airflow range from 30 to 160 L/min). To take into account minor variations of mask resistance at different air pressure, the analytical profile of $R_{\mathrm{II\,mask}}$ as a function of ΔP_{II} was modeled by fitting a first-order polynomial curve on the calculated $R_{\mathrm{II\,mask}}$ data, as previously detailed in [43]. Based on the linear regression model, the values of $R_{\mathrm{I\,mask}}$ were predicted for the ΔP_{I} corresponding to $Q_{\mathrm{I\,tot}}$ equal to 30, 90, and 160 L/min. The predicted $R_{\mathrm{I\,mask}}$ values were then used in (2) to compute the values of $Q_{\mathrm{I\,mask}}$ corresponding to ΔP_{I}. Then, the mask fraction F_{mask}, in agreement with [27], was defined as the fraction of the exhaled airflow passing through the mask filter and was calculated according to the following equation:

$$F_{\mathrm{mask}} = \frac{Q_{\mathrm{I\,mask}}}{Q_{\mathrm{I\,tot}}} = \frac{\Delta P_{\mathrm{I}}}{R_{\mathrm{I\,mask}} \cdot Q_{\mathrm{I\,tot}}}. \tag{5}$$

To characterize the outward TFE of a mask, we finally took into consideration the BFE of the mask filter measured according to the method specified in Annex B of standard EN 14683:2019 [16] using the test rig previously described in [11] and characterized in [42]. Finally, the mask TFE was obtained according to the following equation:

$$\mathrm{TFE} = F_{\mathrm{mask}} \cdot \mathrm{BFE} = \frac{\Delta P_{\mathrm{I}}}{R_{\mathrm{I\,mask}} \cdot Q_{\mathrm{I\,tot}}} \cdot \mathrm{BFE}. \tag{6}$$

E. Face Masks Tested in This Study

The experimental protocol was applied to 50 different face mask models (Fig. A, supplementary material) representative for a range of masks available in the market. The considered models included masks made of woven and/or nonwoven materials, in a range of different designs, varying by the number of filter layers, the filter materials, the filter structure, and the retention system. Specifications of each mask are reported in Table I, including the values of breathability (DP, expressed in Pa/cm^2) and BFE (expressed as %) obtained at our laboratory according, respectively, to the methods defined in Annexes B and C of standard EN 14683:2019 [16], using the equipment previously presented in [11]. Information about the presence of a nosepiece is also listed.

Based on the DP and BFE values, mask models were identified as SMs when compliant to DP and BFE performance requirement set by the standard EN 14683:2019, or, differently, as CMs, as shown in Fig. 3.

TABLE I
MAIN SPECIFICATIONS AND CHARACTERISTICS OF THE CMS AND SMS TESTED IN THIS STUDY

Mask ID	Filter material[a]	N° of filter layers	Structure of filter layers[a]	Filter area (cm^2)	Retention system	Nose piece[a]	BFE[b] (%)	DP[c] (Pa/cm^2)
CM01	PP	3	SMS	169	ear loop, elastic	MW	99.6 (0.3)	69 (12)
CM02	92 % cotton, 8 % PU	2	KK	225	ear loop, elastic	none	91.1 (1.3)	56 (3)
CM03	PP	3	SSS	308	ear loop, elastic	none	93.6 (5.6)	10 (0)
CM04	PP	3	SMS	206	ear loop, elastic	MW	95.1 (4.7)	53 (2)
CM05	PP	3	SMS	196	ear loop, elastic	PO	94.7 (4.6)	30 (2)
CM06	PP	1	S	361	ear loop, elastic	none	90.0 (1.5)	11 (1)
CM07	PP	1	S	356	ear loop, elastic	none	90.6 (2.2)	7 (0)
CM08	92 % cotton, 8 % PU	1	K	241	ear loop, elastic	none	91.2 (1.3)	26 (1)
CM09	100 % cotton	2	KK	208	ear loop, elastic	none	87.0 (1.8)	13 (1)
CM10	93 % cotton, 7 % PU	2	KK	218	ear loop, elastic	none	90.5 (1.4)	34 (4)
CM11	PP	3	SMS	228	ear loop, elastic	MW	99.9 (0.1)	88 (12)
CM12	cotton/PP	3	SWS	280	ear loop, elastic	none	82.6 (1.9)	13 (1)
CM13	PP	1	S	323	ear loop, elastic	none	93.2 (2.9)	11 (1)
CM14	cotton/PP	3	SWS	259	ear loop, elastic	MW	85.4 (1.9)	19 (2)
CM15	cotton/PP	4	SWSS	280	ear loop, elastic	none	92.3 (1.4)	23 (2)
CM16	PP	3	SMS	167	ear loop, elastic	MW	100 (0.1)	63 (20)
CM17	PP	3	SMS	174	ear loop, elastic	MW	100 (0.1)	60 (15)
CM18	PP	3	SSS	201	ear loop, elastic	MW	100 (0.1)	92 (4)
CM19	PP	3	SSS	197	ear loop, elastic	MW	100 (0.1)	71 (3)
CM20	PP	3	SSS	207	ear loop, elastic	MW	100 (0.1)	78 (3)
CM21	100 % polyester	1	W	257	ear loop, adjustable length	none	66.3 (8.4)	41 (2)
SM01	PP	3	SMS	198	ear loop, elastic	MW	99.3 (0.1)	42 (4)
SM02	PP	5	SSMSS	225	ear loop, elastic	MW	99.5 (0.4)	46 (5)
SM03	PP	3	SMS	195	ear loop, elastic	PO	96.8 (0.3)	20 (0)
SM04	PP	3	SMS	182	ear loop, elastic	PO	99.7 (0.3)	30 (2)
SM05	PP	3	NMS	229	ear loop, elastic	MW	99.7 (0.2)	27 (15)
SM06	PP	3	SMS	178	ear loop, elastic	MW	99.8 (0.3)	42 (6)
SM07	PP	3	SMS	170	ear loop, elastic	PO	99.8 (0.1)	39 (2)
SM08	PP	3	SMS	178	ear loop, elastic	MW	95.7 (0.8)	32 (3)
SM09	100 % cotton	1	W	296	ear loop, elastic	MW	98.1 (0.5)	53 (0)
SM10	PP	3	SMS	195	ear loop, elastic	MW	99.7 (0.3)	36 (2)
SM11	PP	3	SMS	194	ear loop, elastic	PO	99.9 (0.1)	20 (1)
SM12	PP	3	SMS	178	ear loop, elastic	MW	99.9 (0.1)	40 (8)
SM13	PP	3	SMS	178	ear loop, elastic	MW	100 (0.1)	58 (26)
SM14	PP	3	SMS	188	ear loop, elastic	PO	100 (0.1)	28 (2)
SM15	PP	1	S	361	ear loop, elastic	none	96.0 (3.6)	12 (2)
SM16	PP	3	SMS	187	ear loop, elastic	MW	99.9 (0.1)	48 (9)
SM17	PP	3	SMS	176	ear loop, elastic	PO	99.9 (0.2)	36 (5)
SM18	PP	3	SMS	189	ear loop, elastic	PO	99.6 (0.3)	23 (4)
SM19	PP	3	SMS	200	ear loop, elastic	MW	100 (0.1)	35 (3)
SM20	PP	2	SS	211	ear loop, elastic	none	99.9 (0.2)	37 (0)
SM21	PP	3	SMS	200	ear loop, elastic	MW	100 (0.1)	30 (3)
SM22	PP	3	SMS	202	ear loop, elastic	MW	100 (0.1)	45 (3)
SM23	PP	3	SMS	158	ear loop, elastic	MW	100 (0.1)	40 (5)
SM24	cotton/PP	4	SMSW	217	ear loop, elastic	none	99.9 (0.2)	44 (1)
SM25	PP	3	SMS	233	head loop	none	99.9 (0.2)	35 (2)
SM26	PP	3	SMS	220	ear loop, not elastic	MW	100 (0.1)	33 (1)
SM27	PP	3	SMS	219	ear loop, not elastic	MW	99.9 (0.2)	36 (4)
SM28	PP	3	SMS	248	head loop	none	99.7 (0.3)	38 (6)
SM29	PP	3	SMS	231	ear loop, elastic	MW	99.8 (0.3)	42 (2)

[a.] Abbreviations; PU: polyurethane; PP: polypropylene; S: spunbonded; M: meltblown, N: polypropylene net, MW: metal wire, PO: polymeric band.

[b.] : BFE: Bacterial filtration efficiency according to Annex B ofEN 14683:2019. Values are expressed as mean (standard deviation) of five replicated measurements.

[c.] DP: Breathability according to Annex A of EN 14683:2019. Values are expressed as mean (standard deviation) of five replicated measurements.

With the aim to understand the impact of the sole nosepiece on TFE, a subgroup of 26 masks, randomly selected among those having a nosepiece, was retested according to the experimental protocol reported above, after removing the metallic or polymeric strip at the nosepiece. The strip was carefully removed by sliding it laterally after having performed a small incision on the external filter layer, without altering other mask design characteristics.

F. Measurement Uncertainty

Measurement uncertainty was addressed according to the guidelines in Joint Committee for Guides in Metrology

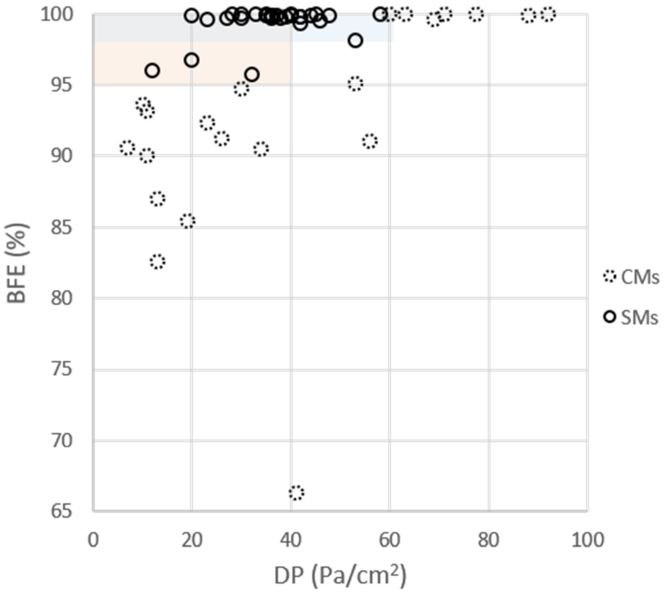

Fig. 3. BFE and DP of the tested masks according to standard EN 14683:2019. Masks models are subgrouped into SMs (solid line circles) when compliant to standard requirement (colored areas: pink for type I and blue for type II-R) and CMs (dashed line circles) when out of standard requirement. Reported values are the mean of five replicated measurements. Dispersions (standard deviations) are listed in Table I.

(JCGM) 100:2008 [50], distinguishing between Type A uncertainty, evaluated by the statistical analysis of series of repeated observations, and Type B uncertainty, evaluated by instrumental accuracy and resolution. The estimator of Type A standard uncertainty for the measurement of any quantity q, directly obtained as the arithmetic mean $\bar{q}$ over N repeated observations q_k, was the standard deviation of the mean $s(\bar{q})$, i.e., the square root of the variance $s^2(q)$ divided by the number of observations

$$u_{\mathrm{A}}(q) = s(\bar{q}) = \sqrt{\frac{s^2(q)}{N}} = \sqrt{\frac{\sum_{k=1}^{N}(\bar{q} - q_k)^2}{N(N-1)}}. \quad (7)$$

Similarly, when the measurement was a predicted value from a linear regression of observations instead of an average, Type A standard uncertainty was obtained by propagating the variances of the slope and the intercept in the interpolant function, dividing by the number of interpolation points, and applying the square root, where slope and intercept variances were calculated by established formulas [50].

Type B standard uncertainty for any measurement derived from DP and airflow rate relied on manufacturer's specifications regarding accuracy of the manometer u_{man} (1% of the read value +1 LSD) and the FM u_{flo} (3% of the read value +1 LSD), respectively. The law of propagation of uncertainty for independent input variables was applied to propagate u_{man} and u_{flo}, and for combining different sources of uncertainty [50].

Experiments of Phase II, measuring $R_{\mathrm{II\ mask}}$ and determining the linear regressor for predicting $R_{\mathrm{I\ mask}}$, were performed once for each mask model. Type A standard uncertainty for the predicted $R_{\mathrm{I\ mask}}$, indicated by $u_{\mathrm{A}}(R_{\mathrm{I\ mask}})$, was computed by propagating slope and intercept variances in the interpolant function. Type B standard uncertainty of $R_{\mathrm{I\ mask}}$, indicated by $u_{\mathrm{B}}(R_{\mathrm{I\ mask}})$, was computed as the average $R_{\mathrm{II\ mask}}$ Type B standard uncertainty $[u_{\mathrm{B}}(R_{\mathrm{II\ mask}})]$ over the 14 measurements, where $u_{\mathrm{B}}(R_{\mathrm{II\ mask}})$ was obtained by propagating u_{man} and u_{flo} in (4)

$$u_{\mathrm{B}}^2(R_{\mathrm{II\ mask}}) = \left(\frac{\Delta P_{\mathrm{II}}}{Q_{\mathrm{II\ mask}}^2}\right)^2 u_{\mathrm{flo}}^2 + \left(\frac{1}{Q_{\mathrm{II\ mask}}}\right)^2 u_{\mathrm{man}}^2. \quad (8)$$

Type A standard uncertainty of BFE, indicated by $u_{\mathrm{A}}(\mathrm{BFE})$, consisted in the standard deviation of the mean over five repeated observations performed according to the method specified in Annex B of standard EN 14683:2019 [16].

The experiments of Phase I for the determination of TFE from ΔP_{I} and $Q_{\mathrm{I\ tot}}$ were performed in quintuplicate by the same researcher for each mask model and flow rate. The mean of TFE over the five replicates ($\overline{\mathrm{TFE}}$) and the standard deviation of the mean $[s(\overline{\mathrm{TFE}})]$, representing the variability from ΔP_{I} and $Q_{\mathrm{I\ tot}}$ observations, were calculated. The overall Type A standard uncertainty of TFE, indicated by $u_{\mathrm{A}}(\mathrm{TFE})$, was then computed combining $s(\overline{\mathrm{TFE}})$ with the Type A contributions from $R_{\mathrm{I\ mask}}$ and BFE propagated in (6)

$$u_{\mathrm{A}}^2(\mathrm{TFE}) = s^2(\overline{\mathrm{TFE}}) + \left(\frac{\Delta P_{\mathrm{I}} \cdot \mathrm{BFE}}{R_{\mathrm{I\ mask}}^2 \cdot Q_{\mathrm{I\ mask}}}\right)^2 u_{\mathrm{A}}^2(R_{\mathrm{I\ mask}}) + \left(\frac{\Delta P_{\mathrm{I}}}{R_{\mathrm{I\ mask}} \cdot Q_{\mathrm{I\ mask}}}\right)^2 u_{\mathrm{A}}^2(\mathrm{BFE}). \quad (9)$$

The overall Type B standard uncertainty for TFE, indicated by $u_{\mathrm{B}}(\mathrm{TFE})$, was computed propagating the instrumental uncertainties (u_{flo} and u_{man}) and Type B contribution of $R_{\mathrm{I\ mask}}$ in (6) according to the following expression:

$$u_{\mathrm{B}}^2(\mathrm{TFE}) = \left(\frac{\Delta P_{\mathrm{I}} \cdot \mathrm{BFE}}{R_{\mathrm{I\ mask}} Q_{\mathrm{I\ mask}}^2}\right)^2 u_{\mathrm{flo}}^2 + \left(\frac{\mathrm{BFE}}{R_{\mathrm{I\ mask}} \cdot Q_{\mathrm{I\ mask}}}\right)^2 u_{\mathrm{man}}^2 + \left(\frac{\Delta P_{\mathrm{I}} \cdot \mathrm{BFE}}{R_{\mathrm{I\ mask}}^2 \cdot Q_{\mathrm{I\ mask}}}\right)^2 u_{\mathrm{B}}^2(R_{\mathrm{I\ mask}}). \quad (10)$$

Finally, the total standard uncertainty for TFE was computed according to

$$u_{\mathrm{tot}}^2(\mathrm{TFE}) = u_{\mathrm{A}}^2(\mathrm{TFE}) + u_{\mathrm{B}}^2(\mathrm{TFE}). \quad (11)$$

G. Statistical Analysis

TFE values were expressed as mean over five replicated experiments and the associated $u_{\mathrm{tot}}(\mathrm{TFE})$. Values of $u_{\mathrm{A}}(\mathrm{TFE})$ and $u_{\mathrm{B}}(\mathrm{TFE})$ were also considered in the interpretation of results.

The results for continuous variables that did not have a normal distribution were presented as median and interquartile interval.

Spearman correlation coefficients were calculated to assess whether a relationship was present between TFE and DP values and between TFE and the mask filter area at flow rates of 30, 90, and 160 L/min.

To investigate the impact of the different design parameters considered in this study, the nonparametric Mann–Whitney U test was used to compare pairs of mask subgroups having different design properties defined by dichotomic variables

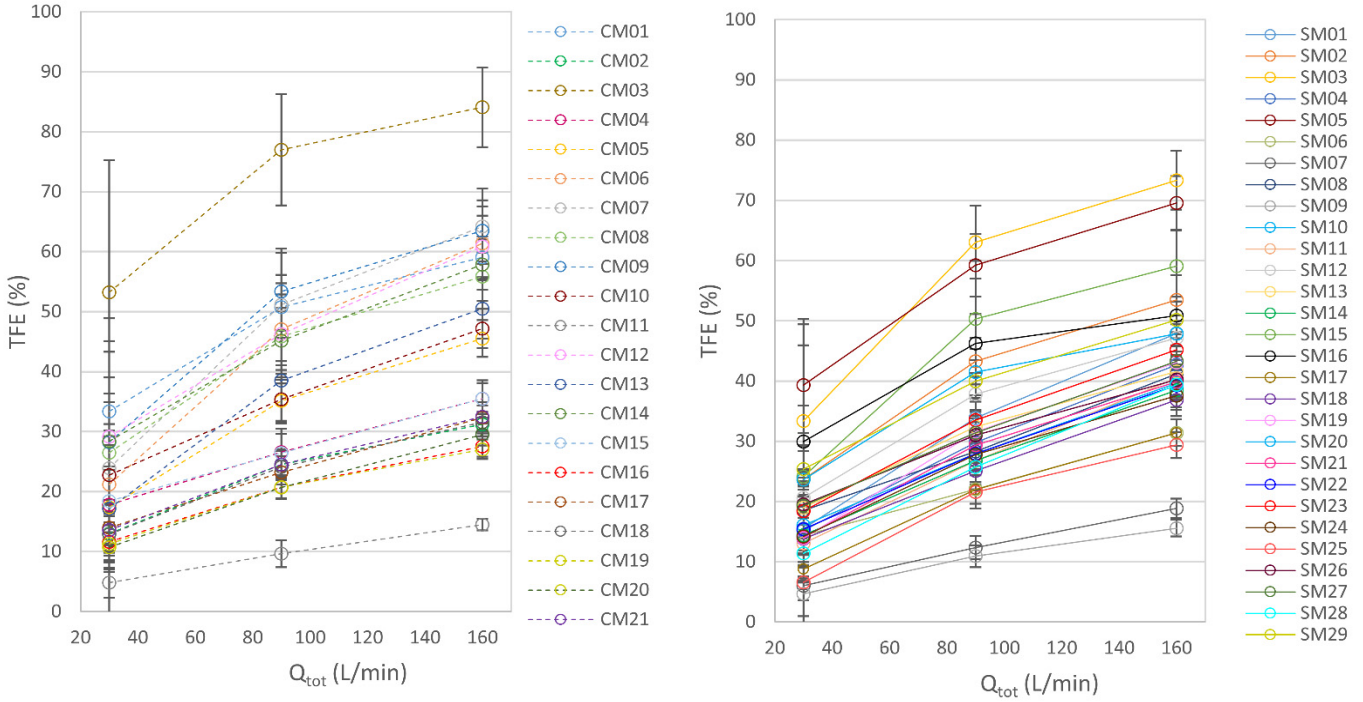

Fig. 4. Percentage of TFE of the tested CMs (dashed line) (left) and the SMs (solid line) (right) in relation to the exhaled airflow rate (Q_{tot}) at 30, 90, and 160 L/min.

(presence/absence of the nosepiece, metallic/polymeric nosepiece, and presence/absence of the meltblown filter layer).

Wilcoxon nonparametric test was used to compare distributions with paired data obtained from testing the subgroup of masks with and without the nosepiece.

All analyses used two-sided tests with a significance level of $p < 0.05$. Statistical analyses were performed using Prism 5 statistical software (GraphPad Software, San Diego, CA, USA).

H. TFE Predictor Model

A response surface method (RSM) [51] was used to model the TFE experimental data. RSM is a collection of mathematical and statistical techniques used in the development of an adequate functional relationship between a response of interest and a number of associated control (or input) variables, called "factors." Using RSM, it is possible to develop empirical polynomial equations relating the response to the factors. This methodology was originally developed to model experimental response [51] and then migrated into the modeling of numerical simulations [52] and observational data [53]. The use of RSM to model observational data was recently summarized in [53]. In our specific case, the factors and their levels were production parameters set by the face mask manufacturers, while the TFE was an experimentally measured output, summarizing mask performance in terms of outward filtration efficacy.

Being TFE expressed as a number ranging 0–1, the following transformation was applied to obtain a normal data distribution:

$$\mathrm{TFE_T} = \arcsin[\sqrt{\mathrm{TFE}}]. \tag{12}$$

The RSM analysis was performed with the programming language R [54] following the statistical strategy and methodological approach described in previous works [55], [56], [57]. Three continuous numerical factors [A-filtering area (cm^2), D-DP (Pa/cm^2), and E-flow rate (L/min)], one discrete numerical factor (B-number of layers), and two categorical factors (F-meltblown and G-nosepiece) were considered.

Since TFE was analytically derived from F_{mask} and BFE, according to (6), we did not consider these two parameters as factors in the model.

The analysis of variance (ANOVA) was used to select the significant terms (having $p < 0.05$) to include in the quadratic model equation having the following general form:

$$\mathrm{TFE_T} = c_0 + \sum_i c_i x_i + \sum_j c_j x_j^2 + \sum_l \sum_l c_{lm} x_l x_m. \tag{13}$$

A quadratic equation was chosen after checking that higher order terms resulted to be aliased and that R^2, the adjusted R^2 (R_A^2), and the predicted R^2 (R_P^2) were maximized, ensuring the minimization of the predicted residual error sum of squares (PRESS). R_A^2 represented the R^2 index adjusted to the numbers of terms inserted in the model (allowing a direct comparison between models with different number of terms), while the R_P^2 indicated how well the regression model predicted responses for new observations. R_P^2 was calculated by excluding one data point from the database, extrapolating the model with the new reduced dataset, and evaluating the ability of the reduced model to predict the excluded datapoint. The process was iteratively repeated for all the datapoints. Similarly, the PRESS was calculated by removing one observation from the dataset and refitting the remaining observations. The out-of-sample predicted value was calculated for the omitted observation in

each case, and the PRESS statistic was calculated as the sum of the squares of all the resulting prediction errors.

The following physical boundary conditions were added outside the range of analysis to guide the empirical prediction of the quadratic model:

$$\text{TFE} = 0 \text{ if } A = 0. \tag{14}$$

According to (14), a set of points with fixed coordinates [Area, DP] = 0, 0 and [Area, DP] = 0, 100 for all the combinations of the categorical and discrete conditions were added to the dataset.

III. Results

A. Total Filtration Efficiency

TFE values obtained at low (30 L/min), medium (90 L/min), and high (160 L/min) outward flowrates are summarized in Table II and graphically depicted in Fig. 4 for each of the 50 tested masks. TFE associated uncertainties (u_{tot}), including Type A (u_A) and Type B components (u_B), are also indicated in Table II.

For sake of clarity, results were grouped by CMs and SMs. Remarkably, TFE values ranged over a large interval (from 5% to 73%) depending on the single mask model and the outward flow rate.

For all tested masks, TFE values systematically increased with the outward flow rates. The median [first quartile; third quartile] values of TFE over the whole tested masks were 17[14; 24]% at 30 L/min, 30[25; 43]% at 90 L/min, and 41[33; 51]% at 160 L/min. No significant differences were found between CMs and SMs subgroups in terms of TFE at the three tested flow rates.

The uncertainty u_{tot}(TFE) associated with each TFE measurement is reported in Table II, including its instrumental and repeatability components. The total TFE uncertainty ranged among all tested masks varied from 2% to 25% at 30 L/min, from 2% to 10% at 90 L/min, and from 1% to 8% at 160 L/min. In general, u_{tot}(TFE) of all tested masks decreased with the increasing of the flow rate applied during the test, with a median [first quartile; third quartile] value of 6[5,8]%, 3[3,5]%, and 3[3,4]%, respectively, at 30, 90, and 160 L/min. When testing low DP masks at low flow rates, u_{tot}(TFE) was generally dominated by the instrumental uncertainty, u_B(TFE).

In these conditions, the instrumental accuracy of the DP measurement system was comparable to the DP itself. Differently, experimental repeatability impacted less on u_{tot}(TFE), with u_A(TFE) ranging from 0% to 3% at 30 L/min, from 0% to 2% at 90 L/min, and from 0% to 3% at 160 L/min.

The correlation analysis between the single design parameters and TFE showed significance only for DP (filter breathability) and the presence of the nosepiece, addressed in detail below, while no correlation with TFE was detected for mask area, the number of layers, and the presence of a meltblown layer.

B. Role of the Mask Filter Breathability

The correlation between TFE values and breathability of the mask filter (DP) is shown in Fig. 5. At all the three tested outward flow rates (30, 90, and 160 L/min), the higher the DP values, the lower the TFE of the mask. Results of the Spearman's test indicated a significant ($p < 0.05$) monotonic negative correlation between TFE and DP. The correlation strength was moderate (Spearman's rho = −0.45 and −0.57 at a flow rate of 30 and 90 L/min, respectively) and strong (Spearman's rho = −0.61 at a flow rate of 160 L/min).

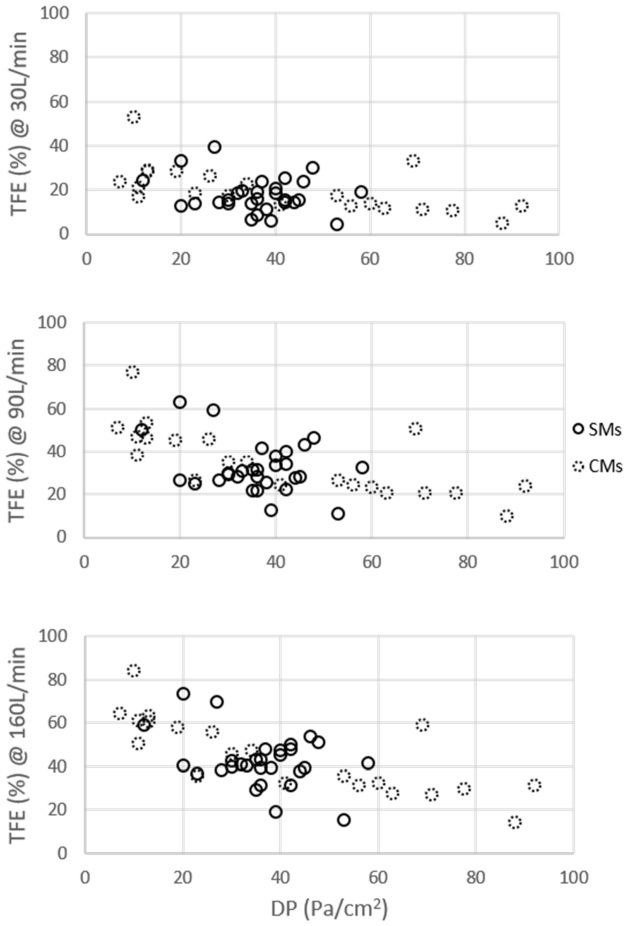

Fig. 5. Scatterplot of the TFE of each mask versus the mask filter breathability (DP). From top to bottom, data are presented for total exhaled airflow rates of 30, 90, and 160 L/min. Dashed circles indicate CMs, while continuous circles indicated SMs.

C. Role of the Nosepiece

Results of the TFE measurements performed on the subset of 26 masks with the original nosepiece installed by the mask manufacturer (w/ NP) and after removal of the nosepiece (w/o NP) are presented as paired measurements in Fig. 6.

Most of 26 tested masks showed lower TFE values without the nosepiece, irrespectively of the outward flow rate. Indeed, the median [first quartile; third quartile] values of TFE measured without nosepiece at the three flow rates were 12[9,15]%, 21[17,29]%, and 32[25,39]%, respectively. With the nosepiece in place, the same group of masks tested in identical testing conditions presented TFE values of 15[13,19]%, 28[22,33]%, and 40[31,45]%. The comparison of TFE values obtained with and without nosepiece over the 26 tested masks indicated that a significant increase in TFE was achieved when the nosepiece was present ($p < 0.05$, Wilcoxon rank-sum test).